ELECTRONIC SUPPLEMENTARY INFORMATION (ESI)

Potassium fertilizer *via* hydrothermal alteration of K-feldspar ore

Davide Ciceri[a], Marcelo de Oliveira[a], Antoine Allanore[a]

[a] Department of Materials Science and Engineering, Massachusetts Institute of Technology, Cambridge MA 02139, USA

ESI 1. PRELIMINARY CONSIDERATIONS ON GREENHOUSE GASES EMISSIONS DERIVING FROM TRANSPORT OF POTASH

A preliminary model is proposed to assess CO_2e emissions due to transport of 1 ton of K_2O from the mines located in Saskatchewan, Canada, to the Cerrado region, Brazil.

It is assumed that a ton of KCl travels:

- A total of 1,600 km by diesel-powered train within Canada, corresponding to the distance between potash mines in Saskatchewan and the port of Vancouver in British Columbia[§].
- A total of 15,729 km (~8,493 nautical miles – 35 days journey) by ocean cargo ship, corresponding to the distance from the port of Vancouver and Port of Santos, São Paulo State, Brazil[‡].
- A total of 2,100 km by truck within Brazil, corresponding to the distance between Port of Santos and Sinop, which is the major agricultural center in the State of Mato Grosso[†].

CO_2e emissions are calculated according to emission factors under two different hypothesis.

- **First hypothesis**

  This hypothesis is based on tabulated values of CO_2e emission as a function of the type of transport used:
  - Transport on Canadian rail[‡]: 0.01785 kg CO_2e t^{-1} km^{-1}
  - Transport on panamax bulk carrier[1]: 0.00536 kg CO_2e t^{-1} km^{-1}
  - Transport on truck (assumed for Brazil to have the same emission factors as in the EU for bulk goods moved on a 24-40 t GCW lorry)[2]: 0.065 kg CO_2e t^{-1} km^{-1}

Under this first hypothesis, the total CO_2e emissions due to transport are 249 kg CO_2e t^{-1}. Assuming that a ton of KCl fertilizer is equivalent to 0.61 t of K_2O, then the equivalent emissions due to transport are 409 kg CO_2e t^{-1}_{K2O}.

- **Second hypothesis**

  This hypothesis is based on tabulated values for fuel consumption and Well-To-Wheel (WTW) CO_2e emission factors, both according to the Global Logistics Emission Council (GLEC)[3].
  - Fuel consumption on train powered by Heavy Fuel Oil (HFO) is 0.005 kg_{fuel} t^{-1} km^{-1} (regional value for North America) at emission factor of 3.42 kg CO_2e kg^{-1}_{fuel} (global value)

---

§ http://www.canpotex.com/what-we-do/logistics

‡ seadistances.org

† Google Maps, Departamento Nacional de Estradas de Rodagem (Brazil)

‡ https://www.cn.ca/en/repository/popups/ghg/ghgcalculatoremissionfactors

- Fuel consumption on container ship powered by Heavy Fuel Oil (HFO) is 0.006 kg_{fuel} t^{-1} km^{-1} (global value) at emission factor of 3.42 kg CO_2e kg^{-1}_{fuel} (global value)
- Fuel consumption on 40t/Class 8 ambient temperature truck by diesel is 0.023 kg_{fuel} t^{-1} km^{-1} (EU value) at emission factor of 3.90 kg CO_2e kg^{-1}_{fuel} (EU value)

Under this second hypothesis, the total CO_2e emissions due to transport are 539 kg CO_2e t^{-1}. Assuming that a ton of KCl fertilizer is equivalent to 0.61 t of K_2O, then the equivalent emissions due to transport are 883 kg CO_2e t^{-1}_{K2O}.

In 2014, Brazil imported 5,291,619 tons of agricultural K_2O[4]. Under the present assumptions and uncertainties, this would correspond to emissions in the order of 2.2Mt CO_2e (first hypothesis) and 4.7Mt CO_2e (second hypothesis). As a term of comparison, the total equivalent emissions due to the entirety[§] of agricultural activities in Brazil corresponded for the same year to 44.2 Mt of CO_2e [4]. Therefore, in Brazil, transport of K_2O alone is comparable to 4.9% to 10.6% of the total agricultural emissions.

[§] CO_2e emissions due to transport of the fertilizers are not included in the total CO_2e emissions

Table ESI 1 Overview of hydrothermal reactivity of CaO-Al_2O_3-SiO_2-H_2O systems.

Reagents	**molar ratios**		***T***	***t***	**solvent**	***S*:*L***	**stirring**	**phases observed**[B]	**reference**
	Al/(Si+Al)	Ca/(Si+Al)	°C	h	-	weight ratio[A]	-	-	-
$Ca(OH)_2$ SiO_2 gel γ-Al_2O_3 (amorphous)	0.67	1.00	150	6	water + KOH	1:10	n/a	$Ca(OH)_2$ hydrogrossular $CaCO_3$	[5]
CaO SiO_2 (amorphous) Al_2O_3 (amorphous)	0.15	0.83	150	0-190	water + NaOH	1:10; 1:5	N	C-S-H 11 Å tobermorite	[6]
CaO coal ash $Al(OH)_3$ or Al_2O_3 (sol)	0.57	0.86	100-180	15	water	1:6	Y	hydrogrossular 11 Å tobermorite $CaCO_3$	[7]
CaO (meta)kaolinite SiO_2 (precipitated) Al_2O_3	0.10-0.13	6.50-1.00	175	0.5-24	water	2:1	N	quartz $Ca(OH)_2$ C-S-H; α-C_2SH 11 Å tobermorite $CaCO_3$	[8]
K-feldspar	0.25	0.22	190-220	20	water + NaOH water + KOH water + $Ca(OH)_2$	1:6	N	altered K-feldspar hydrogrossular C-S-H; C-A-S-H; α-C_2SH tobermorite $CaCO_3$; K_2CO_3; $K_2Ca(CO_3)_2$	[9]
$Ca(OH)_2$ Ultrapotassic syenite	0.24	0.17	200	5	water	1:4	Y	altered K-feldspar hydrogrossular C-A-S-H; α-C_2SH 11 Å tobermorite unidentified carbonates	This study

[A] Assumes a density of 1 g mL^{-1} for all solutions. Values are rounded.

[B] C-A-S-H=non-stoichiometric calcium aluminum silicate hydrate; C-S-H=non-stoichiometric calcium silicate hydrate; α-C_2SH=α-dicalcium silicate hydrate

ESI 2. CALCIUM OXIDE (CaO) CHARACTERIZATION

Despite a controlled storage system, the CaO used in this study (reagent grade, Alfa Aesar) was subjected to a high degree of hydration. An XRD scan showed that the actual composition at the time of the experiment was the following: CaO 5.5 wt%, $Ca(OH)_2$ 93.7 wt%, $CaCO_3$ 0.8 wt%.

According to the manufacturer, the level of impurities in the material as received is as follow:

- 0.005% Cl max
- 0.05% NO_3 max
- 0.1% Fe max
- 0.1% SO_4 max
- Insoluble material: 1.5% max in CH_3COOH and NH_4OH

Trace Metals: (as Pb) 0.01% max

ESI 3. SCHEMATIC OF THE HYDROTHERMAL REACTOR

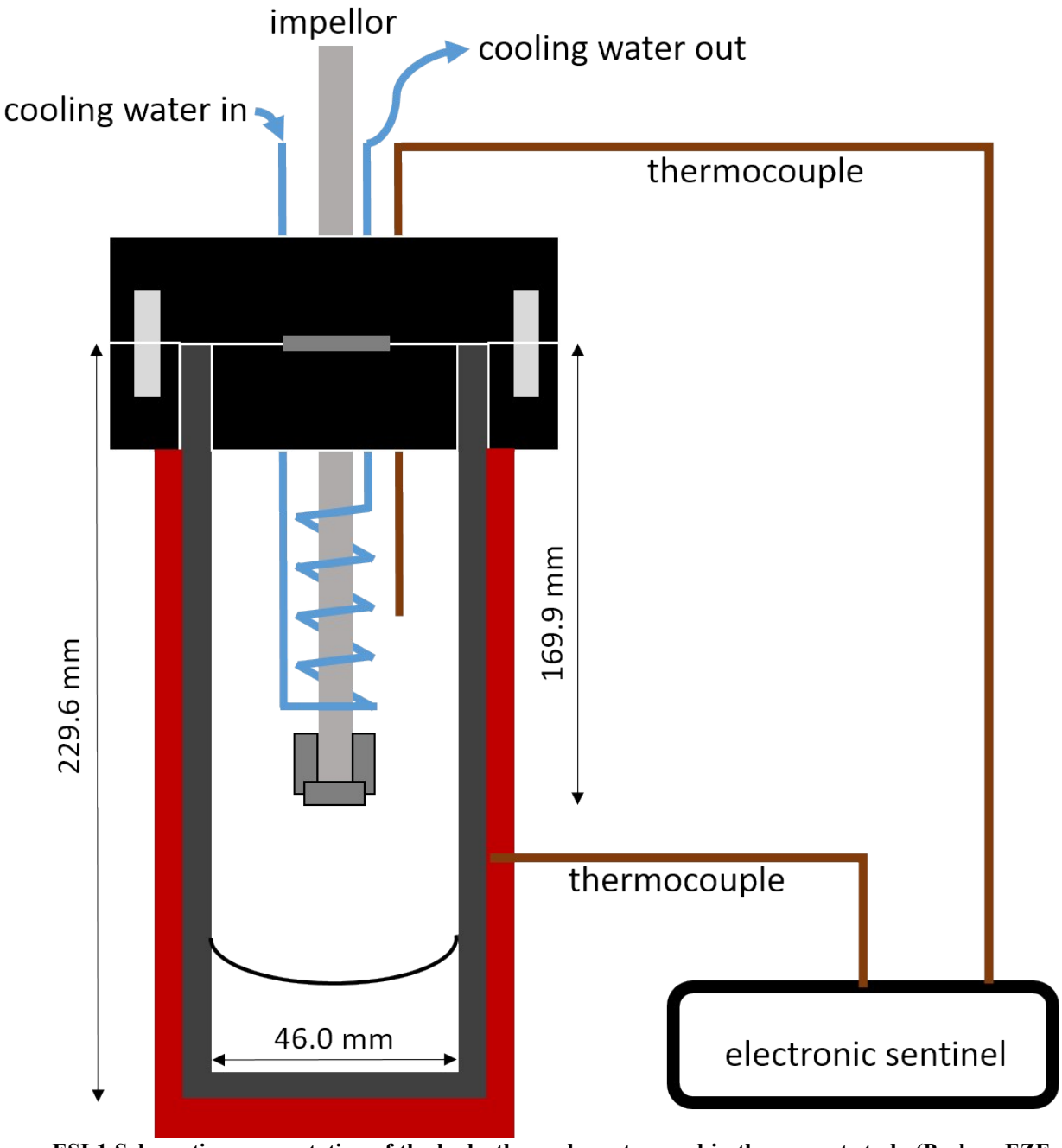

Figure ESI 1 Schematic representation of the hydrothermal reactor used in the present study (Parker, EZE-Seal®, 300 mL). The jacket outside the reactor (depicted in red) is a ceramic heating mantle.

ESI 4. TEMPERATURE VARIATION DURING THE SYNTHESIS OF THE HYDROTHERMAL MATERIAL

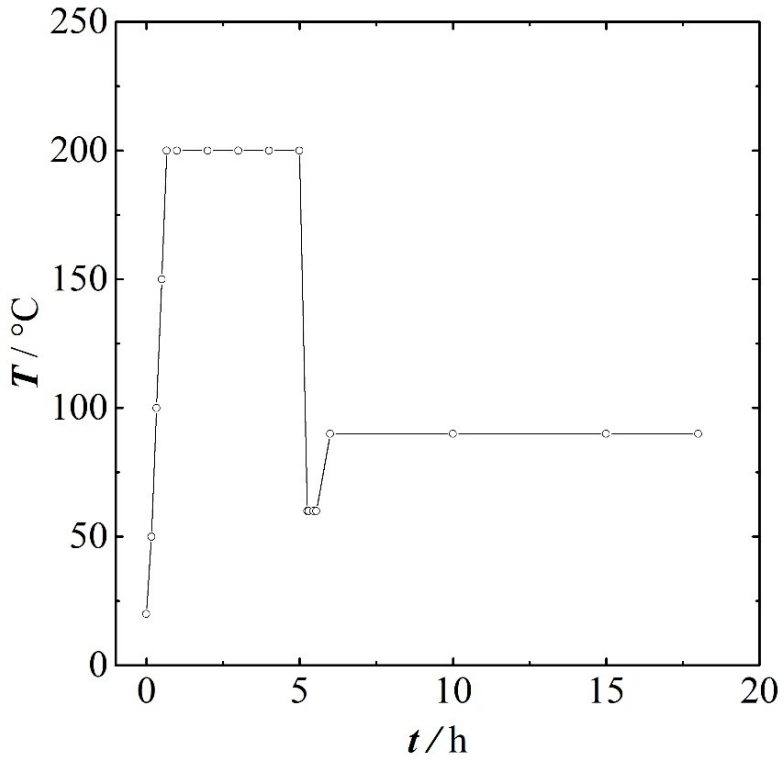

Figure ESI 2 Temperature profile during the processing steps that lead to the hydrothermal material.

ESI 5. APPEARANCE OF THE HYDROTHERMAL MATERIAL

Figure ESI 3 Photographs illustrating the physical appearance of ultrapotassic syenite rock powder (left) and hydrothermal material (right). Both samples showed here are ~2 g. A much more loose packing and possibly a lower density are observed for the hydrothermal material rather than for the ultrapotassic syenite. Actual density measurements were not performed.

ESI 6. CHANGE IN pH DURING LEACHING EXPERIMENTS

Figure ESI 4 shows the variation in pH of a solution of HNO_3 at initial nominal pH=5 upon contact with either the ultrapotassic syenite or the corresponding hydrothermal material. A calibrated pH meter (Hanna, HI 4222) is probing in a beaker the pH of the HNO_3 solution at pH=5 for 5 min, after which a mass of ultrapotassic syenite or hydrothermal material is added under agitation at m_S:m_L=0.1, simulating the conditions of the leaching test. Within a few minutes, the pH of the solution raise to a nominal value of ~6 units in the case of the rock powder, and ~12 units in the case of the hydrothermal material. The system is reactive and the pH never reaches a true chemical equilibrium. In the rock powder as well as in the hydrothermal material, the dissolution of the K-feldspar component alone proceeds indefinetively, until complete tranformation on geological timescales occur. Such processes change the pH of the leaching environment over time.

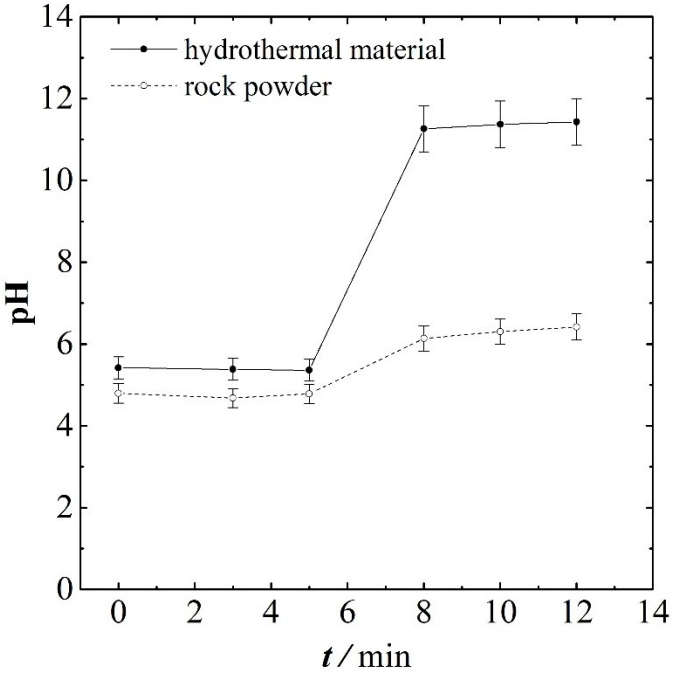

Figure ESI 4 Spontaneous variation of the pH of a solution of HNO_3 at an initial nominal pH=5 contacted with either the rock powder (ultrapotassic syenite) or the hydrothermal material at a m_S:m_L=0.1 and room temperature. The solid is maintained agitated with a magnetic stirrer. Error bars show an arbitrary error of 5%.

ESI 7. X-RAY POWDER DIFFRACTION PATTERN

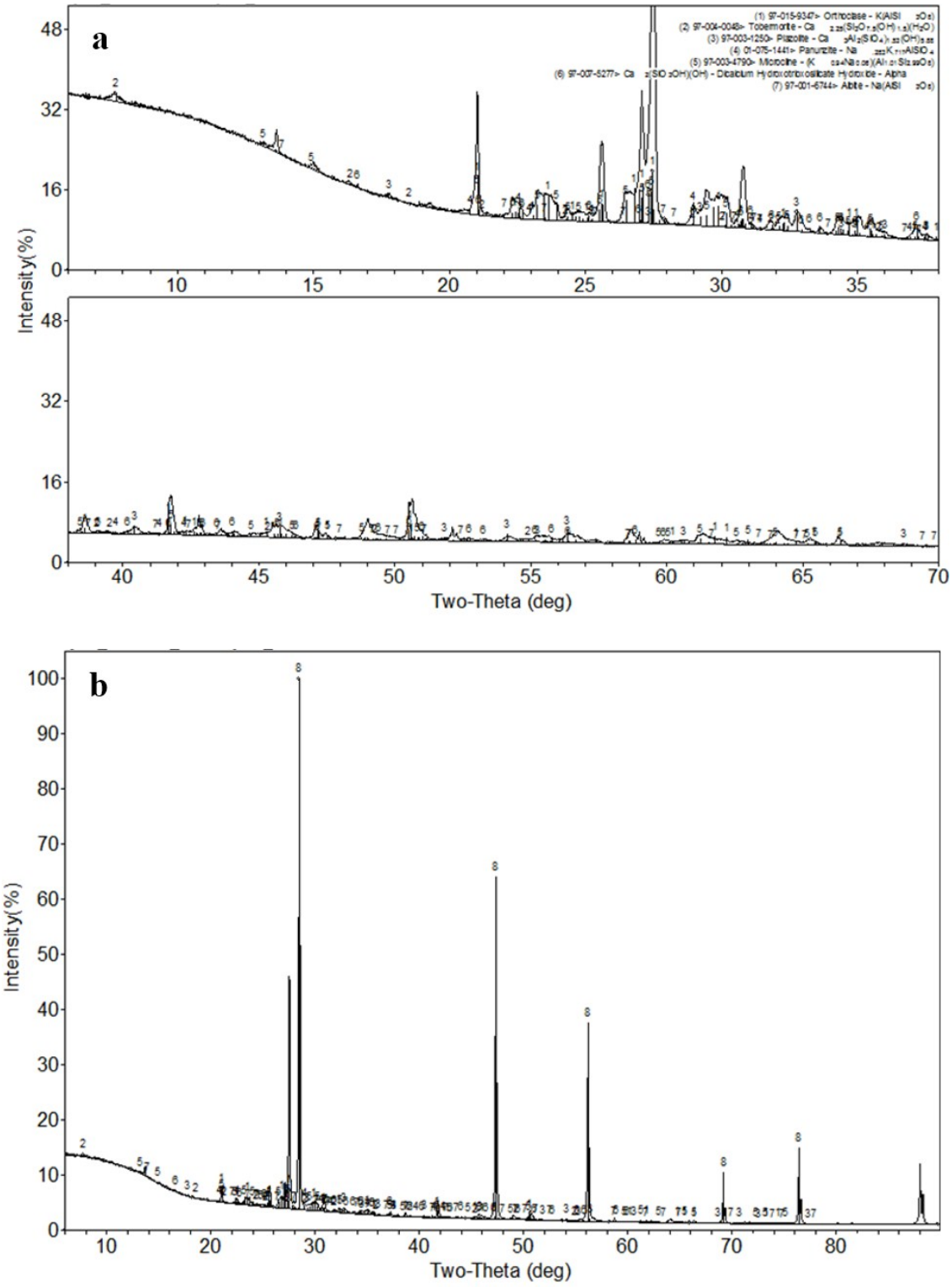

Figure ESI 5 XRD pattern of (a) sample of hydrothermal material as such and (b) sample spiked with 50 wt% of Si (NIST SRM 640) for determination of the amorphous component. Inorganic Crystal Structure Database (ICSD) numbers are as follow: orthoclase (#159347); microcline (#34790); plazolite (#31250); α-dicalcium silicate hydrate (#75277); 11 Å tobermorite (#40048); albite (#16744); panunzite (#30951).

ESI 8. OVERVIEW OF SEM MICROGRAPHS OF THE HYDROTHERMAL MATERIAL

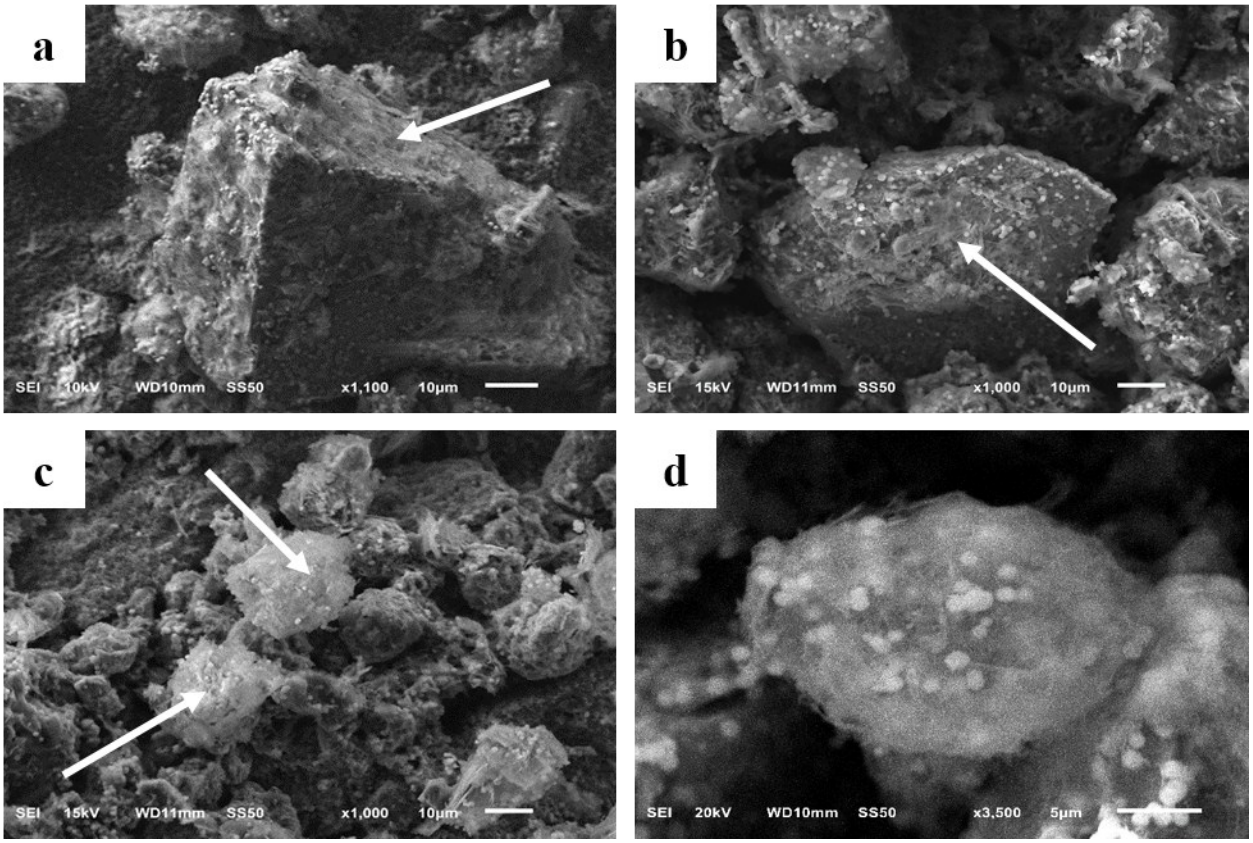

Figure ESI 6 Overview of the hydrothermal material (powder): (a) and (b) altered K-feldspar; round particles of hydrogrossular are clearly visible; the white arrow points at a side of the feldspar surface where fine needles of calcium silicate phases are particularly evident as a moss-like coating (c) white arrows point at round agglomerates (presumably tobermorite); cross sections of such formations are likely to resemble those highlighted in Figure 3b and Figure 3d of the main text (d) close up of one of those formation shown in (c); round particles of hydrogrossular are clearly visible. Images were obtained by dusting a pinch of powder on conductive paint (Carbon Conductive Adhesive 502, Electron Microscopy Sciences).

ESI 9. ELECTRON PROBE MICRO-ANALYZER (EPMA) CHARACTERIZATION OF ULTRAPOTASSIC SYENITE, FEED MIXTURE AND HYDROTHERMAL MATERIAL

An EPMA study was performed on the rock as such, the feed mixture and the hydrothermal material, to understand if ball milling may lead to inclusion of Ca atoms in the feldspar structure. The EPMA experimental protocol was the same described in the main text. All samples are mounted in thin section.

- **Ultrapotassic syenite (thin section)**

Results for MCA41 rock mounted in thin section are reported in ESI-EPMA. The average K_2O content from point analysis was 14.9 wt%, which is in good agreement with the value determined by XRF on the same rock ground in a ball mill (14.3 wt%)[10]. In the feldspar structure of the rock, no Ca was detected, and the total content of oxides neared 100%.

- **Feed mixture**

Results for the feed mixture mounted in thin section are reported in ESI-EPMA. For some of the smallest particles, K-feldspar was enriched in Ca, depleted in K, Si and Al. In general, such an observation does not seem to hold true for bigger K-feldspar grains (> 50 μm). Such findings can be explained according to at least three different hypothesis: i) the Ca detected by EPMA is native to the ultrapotassic syenites; such domains enriched in Ca may break up more easily upon milling, and therefore they are consistently detected in the particles <50 μm. This hypothesis is unlikely given the results discussed above for the rock in thin section. However, note that ball milling has been proved to affect the crystallinity, and possibly also the composition of ultrapotassic syenites as a function of the particles size fraction[5] ii) the energy input during ball milling may activate via mechanical action a process of Ca insertion in K-feldspar iii) Ca is coating the K-feldspar grains, but is not inserted in the crystalline framework. Most likely, a combination of phenomena is actually occurring, and it will be the subject of future investigations.

- **Hydrothermal material**

Selected X-ray elemental maps of the hydrothermal material obtained with EPMA are shown in Figure ESI 7. Specifically, Figure ESI 7(a-c) shows three particles of K-feldspar in three diferent size classes. The small grain is highly depleted in K and enriched in Ca. Al and Si also seem to be particularly depleted with respect to pristine K-feldspar in ultrapotassic syenites. As the particles become bigger such chemical alteration becomes less evident, although a rim of calcium minerals is observed consistently. Note that elemental maps cannot be looked at independently from point analysis (ESI-EPMA). Figure ESI 7(d-f) shows additional selected particles commented in caption.

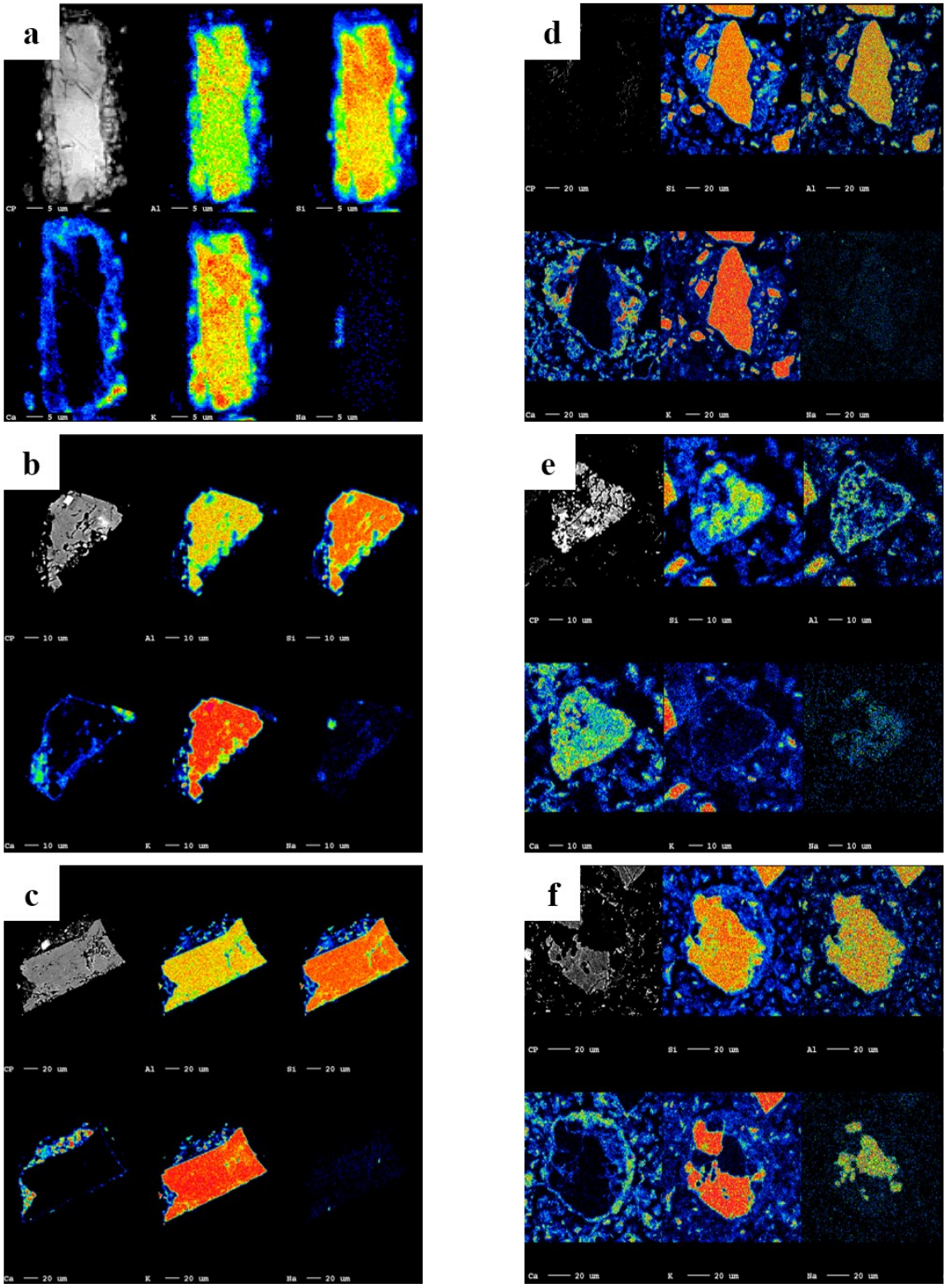

Figure ES1 7 Electron Probe Micro-Analzer (EPMA) X-ray elemental maps. (a) (b) (c) particles of altered K-feldspar in three different size classes, d<50µm, 50<d<100µm and d>100µm, respectively; (d) clump-like formation in the hydrothermal material (compare with Figure 3d of the main text); large mass of hydrogrossular (compare with Figure 3d of the main text); (f) clump-like formation with the central particle of altered K-feldspar containing a distinct inclusion of albite.

ESI 10. ACID-BASE TITRATION OF HYDROTHERMAL MATERIAL

An acid-base titration of the hydrothermal material was carried out as follow:

- First, 0.3 g of hydrothermal material were suspended in 10 mL of DI water under agitation
- Second, standardized 0.1 M HNO_3 (Alfa Aesar) was added to the beaker. After each acid addition (2.5 mL), the system was let to stabilize for 15 min, before the reading was taken. Note that the pH never truly stabilized due to surface reactivity
- Third, the titration curve is plotted as shown in Figure ESI 6, and equivalent points used for back calculations of the base content in the hydrothermal material.

Two distinct equivalent points are observed, at pH=10.0 (3.0 mL) and pH=5.8 (12.0 mL). The first equivalent point can be reasonably attributed to carbonates since the tabulated pKa_2 value for H_2CO_3 is 10.33 (25°C). Differences between experimental and theoretical values may be explained by interferences caused by the surface reactivity of the other mineral phases such as K-feldspar, hydrogrossular and tobermorite. The second equivalent point seems farer from the tabulated pKa_1 value for H_2CO_3, which is 6.35 (25°C). Assuming the first equivalent point is indeed due to carbonates, this would correspond to 0.3 mmol of CO_3^{2-}, equivalent to 4.3 wt% of CO_2 in the hydrothermal material. Such an amount was not detected by XRD, but is in excellent agreement with LOI data (Section 2.2. of the main text). Carbonates were anhedral crystals, but not amorphous, and are not detected by XRD likely because they are below detection limit. If all of the carbonate determined with the titration at the first equivalent point was K_2CO_3, then the expected K leaching test would be 78,000 ppm_K, well-above the experimental data (Figure 5 of the main text). Carbonates in the hydrothermal material are therefore an unidentified mixture, which is likely to comprise K_2CO_3, Na_2CO_3, $MgCO_3$, $CaCO_3$, but possibly also other double carbonate species such as $K_2Ca(CO_3)_2$ (bütschiilite and/or fairchildite)[11]. The second equivalent point does not match the content of carbonate detected at the first equivalent point. Assuming that the second equivalent point is due to the equilibrium $HCO_3^- + H^+ \rightleftharpoons H_2CO_3$, then further to the 0.3 mmol of CO_3^{2-} additional 0.6 mmol of bicarbonate species HCO_3^- must be present originally in the hydrothermal material. Such an amount would correspond to an additional 8.6 wt% of CO_2 content in the hydrothermal material, for a total of 12.9 wt% of CO_2, which is unlikely to be undetected by XRD. We are not able to discriminate if such discrepancies are due to analytical error during titration, analytical error during XRD collection, multitude of carbonaceous species that are all below or near detection limits or strong interference in the titration from other mineral components. Despite such limitations, data point to an effective presence of carbonates in the hydrothermal material.

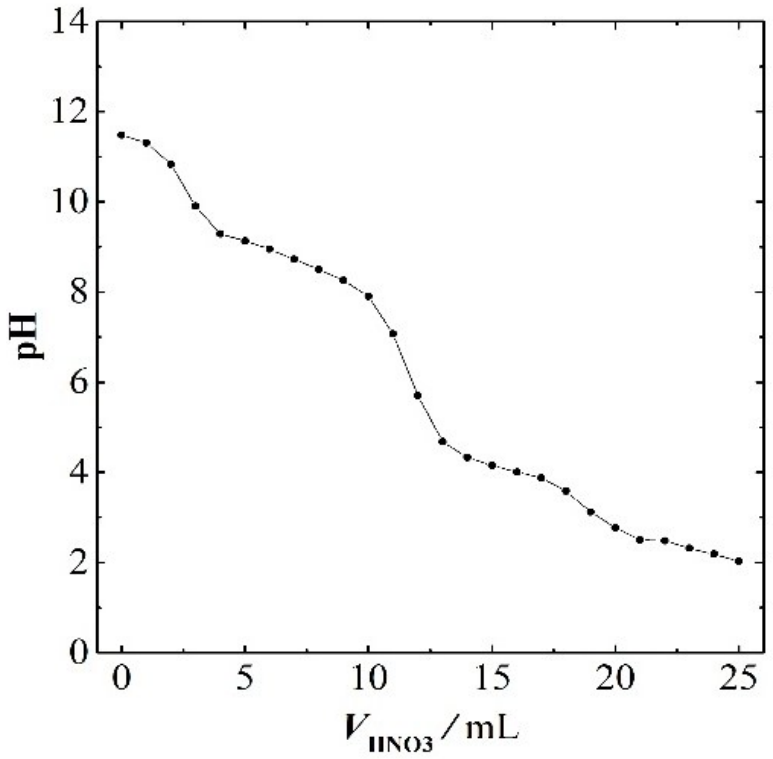

Figure ESI 8 Titration curve of the hydrothermal material (0.3067g) suspended in 25 mL of DI water, with standardized HNO_3 0.1 M (Alfa Aesar).

ESI 11. QUALITATIVE SPOT TEST FOR THE DETERMINATION OF CARBONATES

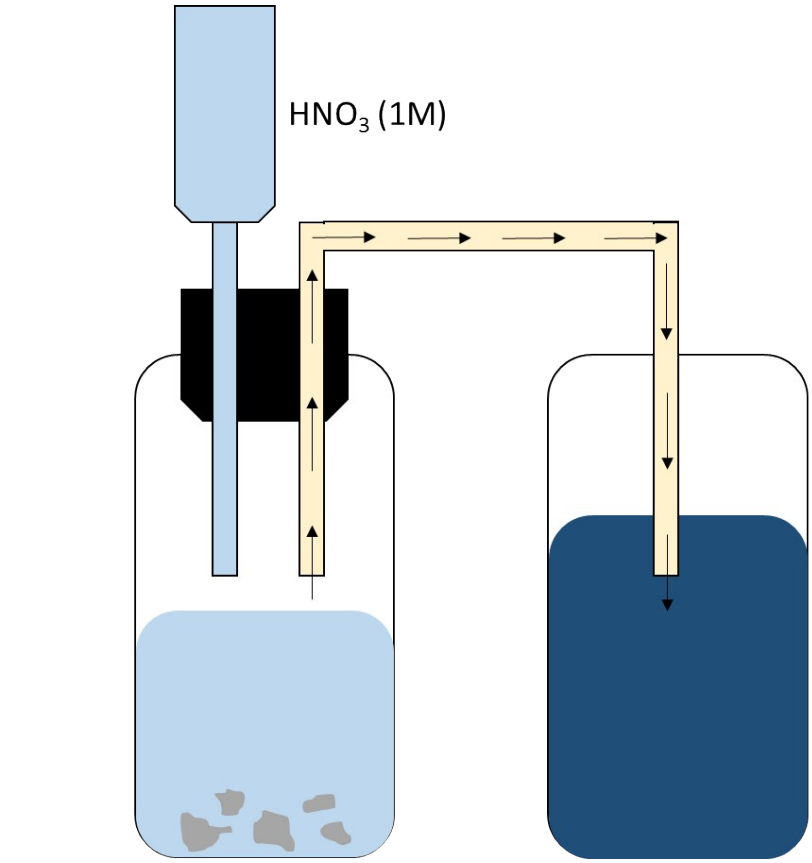

(a)

(b)

(c)

Figure ESI 9 Spot test for the determination of carbonates in the hydrothermal material. (a) Schematic and principle of the experimental apparatus. Concentrated nitric acid (15.6 M) is dropped on top of the material. If carbonates are present, they generate CO_2, which is channeled into a second compartment of the apparatus and precipitated as $BaCO_3$ from a solution of $Ba(OH)_2$ (b) result from a blank test, where the material is ultrapotassic syenite (no $BaCO_3$ is formed) (c) result from a test with the hydrothermal material. A whitish cloud of $BaCO_3$ is formed, confirming the presence of carbonates.

ESI 12. N_2 ADSORPTION/DESORPTION ISOTHERM OF THE HYDROTHERMAL MATERIAL

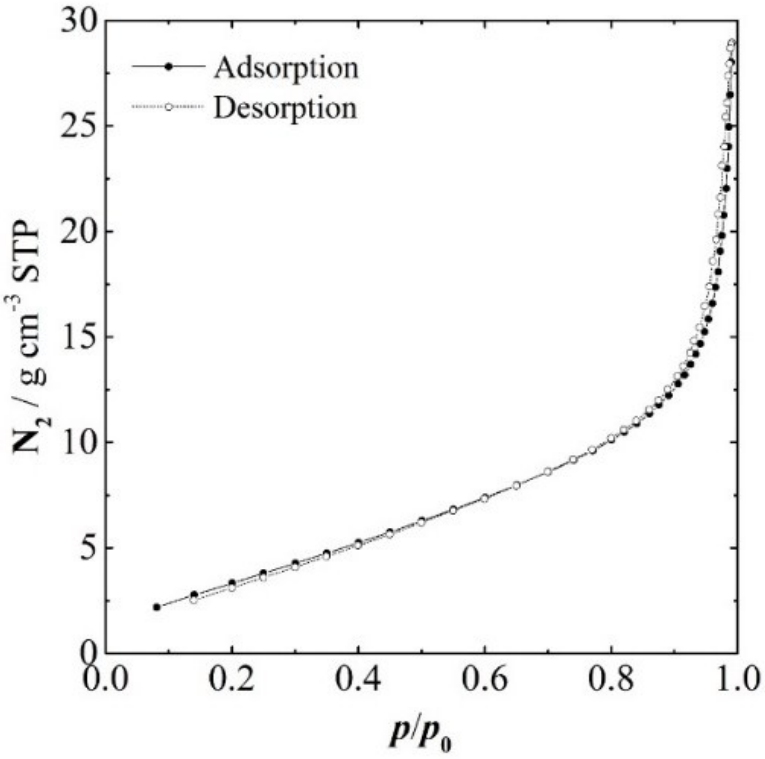

Figure ESI 10 Adsorption and desorption isotherms (-196°C) of N_2 gas at the surface of the hydrothermal material.

ESI 13. MASS BALANCE CONSIDERATIONS

Table ESI2 Overview of data used for mass balance calculations

	K-feldspar (wt %)	K_2O (wt %)	H_2O (wt %)	MM (g/mol)
Ultrapotassic syenite	94.5	14.3	0.1	n/a
K-feldspar	n/a	14.9±0.3	0.0	278.3
Hydrothermal material	66.5	11.7	4.4	n/a
K	n/a	n/a	n/a	39.1
K_2O	n/a	n/a	n/a	94.2

The potassium mass balance was calculated using the data in Table S2, as follow:

- Feed mixture:
    - 21.28 g of ultrapotassic syenite + 3.72 g of CaO
    - K-feldspar equivalent: 20.11 g
    - K equivalent: 2.49 g
    - K_2O equivalent: 3.00 g
- Hydrothermal material:
    - Total mass is 26.1 g
    - K-feldspar equivalent: 17.3 g (measured by XRD; see main text)
    - K-feldspar consumed: 2.8 g or ~16% (equivalent to 0.4 g of K or 0.5 g K_2O)
- Leaching:

  Assume that all K contained in the K-feldspar that was completely converted is fully available in the leaching test. Furthermore, assume that the K available from the remaining altered K-feldspar is negligible. This is justified by considering that the dissolution rate of K-feldspar at pH=12 (ESI S6) reported by Blum[12] is 5.6×10^{-12} mol m^{-2} s^{-1}, corresponding to a range 12.6-189.0 ppm of available K[1].

  Then:
    - Leaching forecast: 15,126±1,976 ppm K (assuming a 1.5% error on XRD)
    - Leaching experimental: 14,065±744 ppm_K, which is within 7% of the calculated value

[1] A specific surface area of 1 or 15 g m^{-2} is assumed for the K-feldspar fraction in the hydrothermal material.

REFERENCES

1 *Minist. Ecol. Sustain. Dev. Energy. French Repub.*, 2012.

2 *Eur. Assoc. Forwarding, Transp. Logist. Cust. Serv.*, 2012.

3 *Smart Freight Centre, 2016. GLEC Framework for Logistics Emissions Methodologies*, Version 1.0. Available from www.smartfreightcentre.org.

4 *Food and Agriculture Organization of the United Nations*., 2016. FAOSTAT statistics database. Rome.

5 H. Maeda, Y. Kurosaki, T. Nakamura, M. Nakayama, E. H. Ishida and T. Kasuga, *Mater. Lett.*, 2014, **131**, 132–134.

6 J.R. Houston, R. S. Maxwell and S. A. Carroll, *Geochem. Trans.*, 2009, **10**, 1.

7 S. Fujita, S. Kenzi and Y. Shibasaki, *J. Mater. Cycles Waste Manag.*, 2002, **4**, 41–45.

8 C.A. Ríos, C. D. Williams and M. A. Fullen, *Appl. Clay Sci.*, 2009, **43**, 228–237.

9 S.K. Liu, C. Han, J. M. Liu and H. Li, *RSC Adv.*, 2015, **5**, 93301–93309.

10 D. Ciceri, M. de Oliveira, R. M. Stokes, T. Skorina and A. Allanore, *Miner. Eng.*, 2017, **102**, 42–57.

11 S. K. Liu, C. Han, J. M. Liu and H. Li, *RSC Adv.*, 2015, **5**, 93301–93309.

12 A. E. Blum, in *Feldspars and their reactions*, Kluwer Academic Publishers, 1st edn., 1994, pp. 595–630.